



Contract No. NMP3-CA-2008-218696-ECONAM

Electromagnetic Characterization of NAnostructured Materials

DELIVERABLE D2.1.6

**OVERVIEW OF THE STATE-OF-THE-ART AND MOST PROMISING
MEASUREMENT TECHNIQUES**

**CONSOLIDATED REPORT ON DELIVERABLES 2.1.1-2.1.5
COMPLEMENTED BY THE LATEST UPDATES**

Due date of deliverable: T0+ 35 months

Actual delivery date: 26 February 2011

Leading contractors: QUB, KIT, UoG, Aalto

Project co-funded by the European Commission within the Seventh Framework Programme (2007-2013)		
Dissemination Level		
PU	Public	PU
PP	Restricted to other programme participants (including the Commission Services)	
RE	Restricted to a group specified by the consortium (including the Commission Services)	
CO	Confidential, only for members of the consortium (including the Commission Services)	

Table of contents

Table of contents	2
Summary	3
Experimental Characterization of Metamaterials.....	4
1. Introduction	4
2. Linear characterization of metamaterials	5
2.1. The ideal measurement.....	5
2.2. Optical measurement techniques.....	6
2.3. Recent advances in measurement techniques	7
2.3. Instrumental limitations.....	10
3. State-of-the-art in experimental characterisation of metamaterials	11
3.1. Structures with inversion symmetry along the surface normal.....	11
3.2. Structures with no centre of inversion along the surface normal	12
3.3. Interferometric experiments	13
3.4. Oblique incidence	13
3.5. Chiral metamaterials	13
3.6. On measurements of the effective refractive index.....	14
4. Concluding Remarks.....	15
References	15

Summary

Most techniques employed for evaluating the electromagnetic parameters of metamaterials are based upon transmission and reflection measurements, often followed by post-processing to retrieve the real and imaginary parts of dielectric permittivity ϵ and magnetic permeability μ . The phase information of the scattered fields (S-parameters) is essential for an adequate retrieval of ϵ and μ . However, the phase is more difficult to obtain at optical frequencies than in the microwave range, and therefore alternative schemes have been developed. For some experiments, full-wave simulations of the test structures are used for achieving the ultimate goal of the ϵ and μ retrieval. The normalised S-parameters obtained from the simulations are then used to extract ϵ and μ via the Fresnel equationsⁱ, often with the simplifying assumptions. Techniques for retrieving the phase include the use of phase masksⁱⁱ, angular resolved measurementsⁱⁱⁱ, and ellipsometry^{iv} where the ratio of TM-to-TE polarized light is plotted as a function of frequency at oblique incidence - and femto-second laser interferometry,^v where the group and phase velocities are obtained from interferograms. The main approaches to the experimental characterization of metamaterials at optical wavelengths as well as in microwave and THz ranges are reviewed here.

ⁱ Spectroscopy of metamaterials from infrared to optical frequencies, W. J. Padilla, D. R. Smith, D. N. Basov, J. Opt. Soc. Am. B Vol. 23, No. 3 pp404-414 (2006)

ⁱⁱ Experimental Demonstration of Near-Infrared Negative-Index Metamaterials, S. Zhang, W. Fan, N. C. Panoiu, K. J. Malloy, R. M. Osgood, and S. R. J. Brueck, PRL 95, 137404 (2005)

ⁱⁱⁱ A. J. Hoffman, L. Alekseyev, S. S. Howard, K. J. Franz, D. Wasserman, V. A. Podolskiy, E. E. Narimanov, D. L. Sivco and C. Gmachl, Nature Materials Vol 6 pp946-950 (2007)

^{iv} Terahertz Magnetic Response from Artificial Materials, T. J. Yen, W. J. Padilla, N. Fang, D. C. Vier, D. R. Smith, J. B. Pendry, D. N. Basov, and X. Zhang, Vol 303 Science pp1494-1496 (2004)

^v Simultaneous Negative Phase and Group Velocity of Light in a Metamaterial, G. Dolling, C. Enkrich, M. Wegener, C. M. Soukoulis, S. Linden, Science Vol 312 pp892-894 (2006)

Experimental Characterization of Nanostructured Materials

1. Introduction

The field of artificial and nanostructured electromagnetic materials has seen rapid and expansive growth in recent years. As the new and emerging materials advance and become increasingly complex, both the measurement techniques and the material parameter evaluation procedures also evolve to ensure the physically meaningful characterisation and description of the observed phenomena. The integrity and quality of these measurements are of utmost importance here, and therefore it is essential that the appropriate measurement techniques are employed for evaluating the extrinsic response and testing the intrinsic properties of material specimens.

This literature review covers the main aspects of the experimental characterisation of artificial and nanostructured materials and the required measurement techniques. In particular, the works concerning, amongst other areas, three-dimensional metamaterials, optical incidences, bi-anisotropic structures, retrieval of intrinsic properties of materials and nanostructures are overviewed.

Before directly addressing the metamaterial characterization issues, it is necessary to remark that the notion “optical wavelengths” is generally not strictly defined and has often been misused, aiming at suggesting to laymen wavelengths in the visible part of the electromagnetic spectrum. Here, in agreement with a bulk of literature, we define “optical wavelengths” as wavelengths of just a few micrometers, equivalent to about 100 THz frequency of light and above. At yet lower frequencies, approaching the far-infrared (or “THz regime”), the issues of sample characterization tend to be somewhat different from the optical regime. The visible part of the optical spectrum is between approximately 400 THz (red) to 790 THz (blue) or from 390 nm (blue) to 760 nm (red). In general optical range is associated with electromagnetic radiation that can be influenced by lenses and gratings and incorporates the ultra-violet, visible and infra-red regions of the spectrum. At frequencies higher than the visible light, the required inhomogeneity scale becomes too small to be technologically achievable at present, and there are no artificial electromagnetic materials that would function at ultra-violet frequencies.

Also it is instructive to briefly recall how today’s state-of-the-art metamaterials at optical frequencies look like – as this aspect poses certain constraints on the characterization process. The vast majority of metamaterial structures have been made via serial, hence time-consuming, lithographic approaches (e.g., electron-beam lithography, focused-ion-beam lithography, or direct laser writing). As a result, typical sample footprints are only of the order of $100 \times 100 \mu\text{m}^2$. This limited sample size, with respect to the source and detector area at shorter wavelength of measurement leads to use of focusing lenses and the unavoidable averaging of the measurements. This is further discussed in Section 2.3. Rather recent brief [1]-[2] and comprehensive [3] reviews of the corresponding magnetic and/or negative-index metamaterials can be found in the literature. Examples of notable exceptions are metamaterials made via holographic lithography [4]-[5] or via nano-imprint techniques [6]. The footprint of the latter specimens is of the order of square-centimetres. Yet much larger footprints can be realized along these lines in the future, and there are attempts to use some self-assembly techniques to fabricate metamaterial structures [7]-[9].

Furthermore, the vast majority of metamaterials at optical wavelengths demonstrated experimentally thus far contain only a single functional layer [1]-[3], which can contain more than one physical layer. Notable recent experimental exceptions are a three-functional-layer negative-index metamaterial at 1.4- μm wavelength [10], a four-functional-layer magnetic metamaterial at 3.7- μm wavelength [11], and a ten-functional-layer negative-index metamaterial at 1.8- μm wavelength [12]. All of these have a total thickness significantly less than one wavelength of light

in the free space. Interesting metal-insulator-metal slot waveguide structures supporting backward waves over many wavelengths of light along the propagation direction in the waveguide plane have also been reported [13]-[14]. However, their optical characterization is not discussed here as such waveguides are not classified as “metamaterials”. There has recently been a concerted effort to push the magnetic frequency response of metamaterials deeper into the visible range of the electromagnetic spectrum. Previous work has shown that simply scaling the size of metamaterial structures, such as split ring resonators (SRRs), only continues to decrease the wavelength of the LC resonance peak up to a certain threshold [15]. Therefore continually making structures smaller in size will not result in the resonance being shifted further and deeper into the visible range.

It is important to note that all the actually fabricated metamaterial structures published to date are anisotropic, often they are even biaxial. Also, the low symmetry of most artificial structures generally allows for strong polarization sensitivity. These geometric and spatial dependences in the metamaterial parameters further complicate the measurements and analysis by effectively multiplying the problem for the number of unique directions. Furthermore, essentially all metamaterial structures are physically supported by some kind of a dielectric substrate – an aspect, which has to be accounted for in the characterization process as well.

An EU sponsored publication [16] covers the basic electromagnetic theory and fabrication methods employed for manufacturing of nanostructured materials.

2. Linear characterization of metamaterials

The experimental characterisation of metamaterials is predominantly based upon the measurements of the scattering parameters of specimens illuminated by plane electromagnetic waves in optical, THz and microwave spectral ranges. Therefore, the acquired data are dependant on the angle of incident light and polarization, while most measurements are limited to normal incidence. For measurements using an oblique incidence, the specimens would usually comprise multiple functional layers rather than a single layer structure, which poses numerous fabrication difficulties. For these reasons most experimental works use light at normal incidence.

Additionally, it occasionally is necessary to perform experiments that distinctly measure the electromagnetic interaction between individual constituent elements and particles in the arrays representing the artificial material. Parameters such as the separation distance between structures and layout configurations and geometries have been shown to influence the coupling effects [17], the importance of which has been documented in [18]. For these purposes, near field optical spectroscopy is usually used. Alternatively, a sensitive spatial modulation technique based upon the experimental measurements of the extinction cross-section spectrum has recently been demonstrated for SRR dimmers at near-infrared frequencies.

2.1. The ideal measurement

The conceptually perfect experiment on a periodic metamaterial with regular sub-wavelength lattice constant can provide measurements of the frequency-dependent complex reflectance and transmittance coefficients of the sample at all incidence angles and polarizations of the impinging ideal monochromatic plane wave. Furthermore, this ideal measurement should include the (generally elliptical) polarization state of light scattered by the sample. Clearly, in linear optics, frequency-domain information can equivalently be expressed in the time-domain, where “complex” translates into amplitude and phase of the wave. For imperfect or for (intentionally) non-periodic or nonuniform structures, scattering of light into the entire solid angle may occur because the material properties vary across the sample. In the ideal experiment this scattering should be characterized completely for all solid angles.

The raw data acquired in these experiments are subject to further post-processing. However, it is important to emphasise that anything beyond the specific measured quantities, e.g., retrieval of whatever *effective* optical parameters (refractive index, impedance, dielectric permittivity,

magnetic permeability, bi-anisotropy parameter, etc.), is *not* a subject of the experimental optical characterization procedure itself but a subject of *interpretation* (!) of the acquired experimental data. This distinct step – which is interlinked with the parameter retrieval through the theoretical models or numerical simulations – will be briefly discussed in Section 3 below. The issues of nonlinear metamaterial characterisation, for example those with gain, are beyond the scope of this review.

2.2. Optical measurement techniques

The basic optical measurements (which typically do not provide phase information) can be performed in many analytical laboratories. However the standard instruments may need some modifications to accommodate samples of small size – typically with addition of a microscope optically coupled to the measurement system. The typical setup includes grating spectrometer, in which a broadband light source illuminates slits and light impinges onto a grating which selects only a narrow band of light. Fourier Transform Spectrometer (schematically shown in Figure 1) and broad-band ellipsometers in which polarised light is incident at an angle to the substrate surface and the subsequent reflected beam’s polarisation state is measured (see Figure 2). Some systems allow both transmission and reflection measurements by simple reconfiguration, ellipsometers typically allow the angle of incidence to be varied. However, most commercial spectrometers do not allow the angle of incidence to be varied.

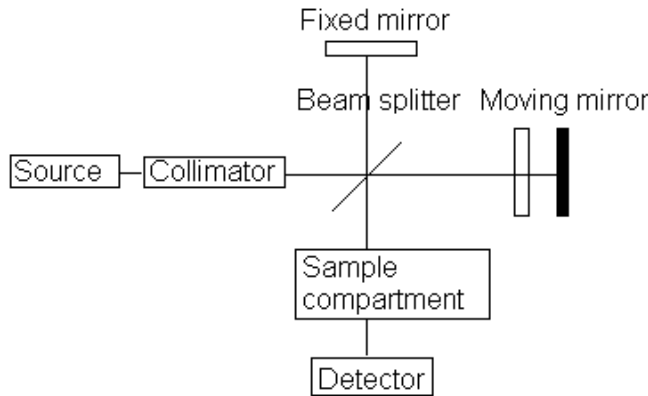


Figure 1: Schematic diagram of a Fourier transform Spectrometer. The interference pattern at the detector is obtained by moving the mirror and changing the optical path length. When a sample is present the interference pattern, as a function of path difference, is modulated by the presence of absorption bands in the sample. The interference pattern is then ‘Fourier transformed’ to give the absorption (or reflection/transmission) as a function of wave number and obtain a spectrum [19].

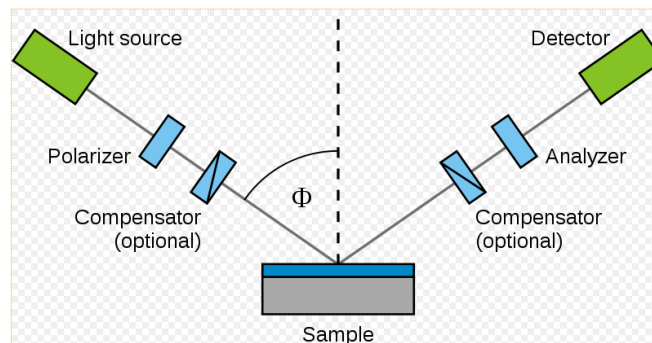


Figure 2: Schematic diagram of an ellipsometer [20].

Similarly Time Domain Spectroscopy (TDS) in which the phase angle of the measurement is obtained from interference methods are usually custom built systems. A simplified schematic of a TDS is shown below in Figure 3. The illuminating EM radiation is generated by the femtosecond pulses from a Ti Sapphire laser incident on either a crystal converter or optoelectronic converter to produce for example THz radiation. The optical delay line alters the phase of the beam arriving at the sample. A detailed introduction is given in reference [21].

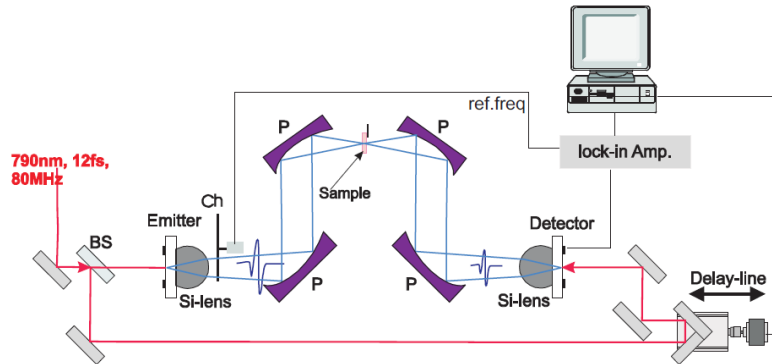


Figure 3: Schematic diagram of Time Domain Spectroscopy setup [21]

2.3. Recent advances in measurement techniques

Although no new fundamental ways for metamaterial measurements have been discovered yet, significant progress in S-parameter measurement techniques, particularly in relation to the phase measurements across the spectrum from visible to microwave region, and optical field measurements have been reported recently.

2.3.1. An experimental method for broadband phase measurements based upon a white-light Fourier-transform spectral interferometer was implemented in [22]. The experimental setup is a Jamin–Lebedeff interferometer modified for the transmission and reflection measurements at normal incidence. The measured data are used to determine the dispersion relation of metamaterials at normal incidence in terms of the complex wavenumber that leads to retrieval of an effective refractive index. Using this approach the refractive index error $\sim 4\%$ in the real and imaginary parts can be achieved.

The measurements were performed with a supercontinuum light source (spectral bandwidth $0.4\mu\text{m}$ – $1.7\mu\text{m}$). After a collimator and a polarizer, the linear polarized light passes a calcite beam displacer, where the beam is divided into two parallel, orthogonally polarized beams with a displacement of 4 mm. These two beams represent the two arms of the interferometer. In the configuration for the transmission phase measurements the beams traverse the sample and then pass an achromatic half-wave plate, which rotates the polarization in each beam fo 90° . The two beams are recombined in the second beam displacer. As the beams in the interferometer arms are orthogonally polarized, the interference between them can be obtained using another linear polarizer. Finally, the light is collected into a photonic crystal (PhC) single-mode fibre and measured with an optical spectrum analyzer.

2.3.2. THz-Time Domain Spectroscopy (TDS) normally requires two measurements [23]: (i) the waveform is measured for the known reference dielectric material, and (ii) the measurement is made with the test sample. By virtue of reasonably clear separation in time between the main transmitted pulse and the first internal reflection, it is possible to extract only the first directly transmitted THz pulse. Comparing the magnitude ratio and phase discrepancy between the test and reference samples, the real and imaginary parts of the effective refractive index of the

sample can be retrieved simultaneously. A detailed retrieval procedure enables one to extract the negative refractive index of low-loss metamaterials based on THz-TDS measurements [23]. The method provides a direct and simple way to probe the real part and imaginary part of refractive index of metamaterials. Its validity has been demonstrated through theoretical simulations on several typical cases.

2.3.3. At optical frequencies, it is very difficult with the current technology to measure directly the electric and magnetic fields of electromagnetic wave in real time as one cannot measure amplitudes and phases within a single wavelength. Therefore indirect approaches have been developed to obtain the spatial profiles of the guided modes in nanostructured materials. For example, the spatial profiles of all modes have been obtained using spatial Fourier transforms applied to periodic PhC with arbitrary combination of propagating and evanescent waves [24].

The lateral electromagnetic coupling and the corresponding spatial profiles of resonances in SRR dimmers [25] and gold nanoparticles [26] have been obtained by measuring the extinction cross section spectrum and optical absorption. In [25] the extinction cross-section spectrum of SRR dimmers (SRRs aligned in various formations) has been measured at near-infrared frequencies using a sensitive spatial modulation technique. By applying Lorentzian fits to the measured data the resonance frequency, extinction cross-section spectral peak and quality factor were derived. The approach used for the spectral measurements is of primary interest here. A schematic of the spatial modulation setup is shown in Figure 4. A white laser beam is passed through a grating monochromator with a resolution of 1nm, filtering the spectrum, before being spatially filtered by a single-mode optical fibre. The output from this fibre is then projected onto the sample to be measured by both a plano-convex and a convex lens separated by a polarizer, thus ensuring linear polarisation of incident light. A piezoelectric tilt mirror is positioned in front of the polariser to modulate the lateral position of the Gaussian beam so that it is on the same plane as the sample, which is itself mounted on a Piezo stage. An InGaAs detector directly connected to a lock-in amplifier is used to detect the light transmitted through the sample.

This is one of the applications of this type of experimental measurement setup. As already mentioned, in the earlier study this technique was utilised to measure the optical absorption of gold nanoparticles, some with a diameter as small as 5nm [26].

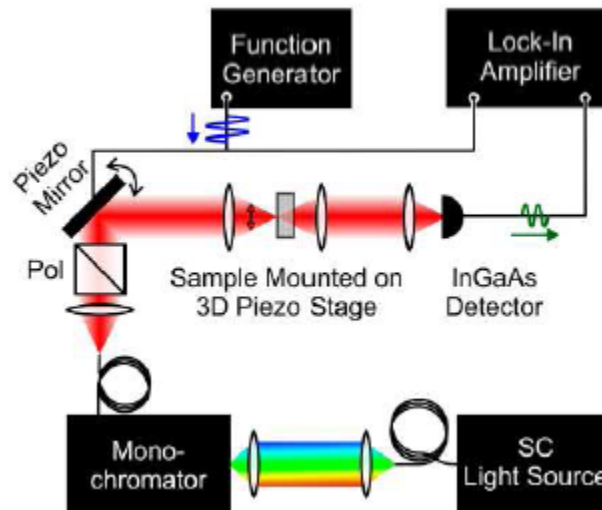


Figure 4: A schematic of the experimental spatial modulation equipment setup [25].

2.3.4. Direct mapping of the electromagnetic near-fields in metamaterials has recently been reported in [27]. Using experimental setup shown in Fig. 5, the authors measure the amplitude,

phase and polarization of the electric field from a metamaterial made of SRR arrays. Photoconductive antennas emit THz pulses which are optically gated by a connected mode-locked laser. The resultant beam is then imaged onto the metamaterials sample, behind which is a silicon-on-sapphire detector chip. Raster scanning the detector chip, which sits at a distance of $30\mu\text{m}$ from the sample surface, allows the THz electric near-field to be spatially resolved. This is made possible by a $10\mu\text{m}$ photoconductive gap that lies between H-shaped electrodes that sit on the surface of the silicon. The SRRs on the sample must be positioned closely to the detector electrodes for measurements to be taken. A detailed schematic of the terahertz near-field system and a cutaway profile of the sample and detector chip are shown in Fig. 5 below.

It is noteworthy, that this approach has only been applied to structures in the low terahertz range. The SRRs used in this experiment each had a typical footprint of $500\mu\text{m}$ by $500\mu\text{m}$. Nevertheless it is claimed in [27] that this is a rare experimental study in a field dominated by simulation based measurements.

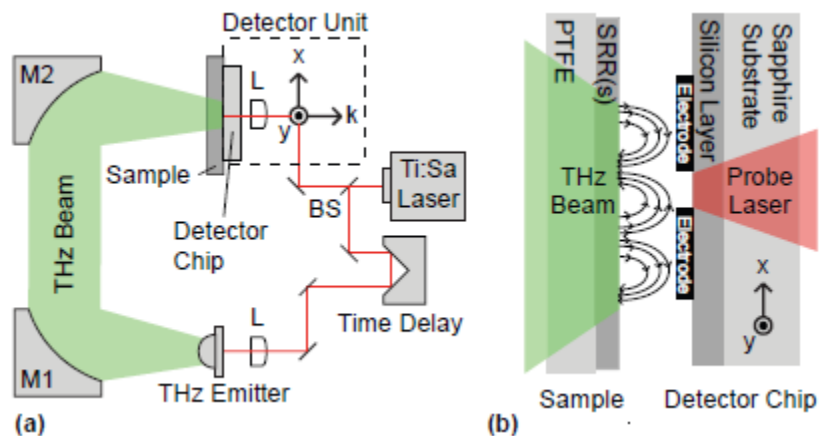


Figure 5: (a) Experimental equipment configuration containing a mode-locked laser, beam splitter, lenses, THz emitter, mirrors and detector unit. (b) A cross section of a sample under investigation and the detector chip [27].

2.3.5. A novel perspective on optical measurement - the probing of light itself, has been reported in [28]. The experimental setup intended to visualise the electric and, more interestingly, the magnetic field distribution of propagating light is shown in Fig. 6. A near-field aperture probe with a diameter of 230nm is used to raster-scan the sample Si_3N_4 waveguide which is connected to linearly polarised laser light with a wavelength of 1550nm . The probe is positioned only 20nm above the sample, allowing the retrieval of the evanescent field of the light. The output from the probe is then connected to a reference beam of light, which is laterally split by a polarizing beam splitter for separate detection of electric and magnetic fields. For the magnetic field to be probed and measured, it must first be converted to an electric field so that it can be measured by the detector. This is accomplished by creating a 40nm crevice in the tip of the probe for optical bi-anisotropy to be exhibited. Because the split is far smaller than the wavelengths of the visible spectrum, electric field signals are suppressed. A similar near-field study into magnetic responses, this time when applied to SRRs, has also been conducted in [29].

Despite the fact that such experiments are reliant on interpretation and occasionally modelling of the data acquired, they can prove useful for future advances in optical characterisation. The work detailed in [28] has potential to be of particular benefit for characterisation of metamaterials.

The papers cited discuss various aspects of measurement of a specific nanostructure or metamaterial. Even though some works are based on simulated experiments, they provide insight in the directions where nanostructure fabrication and characterisation are progressing.

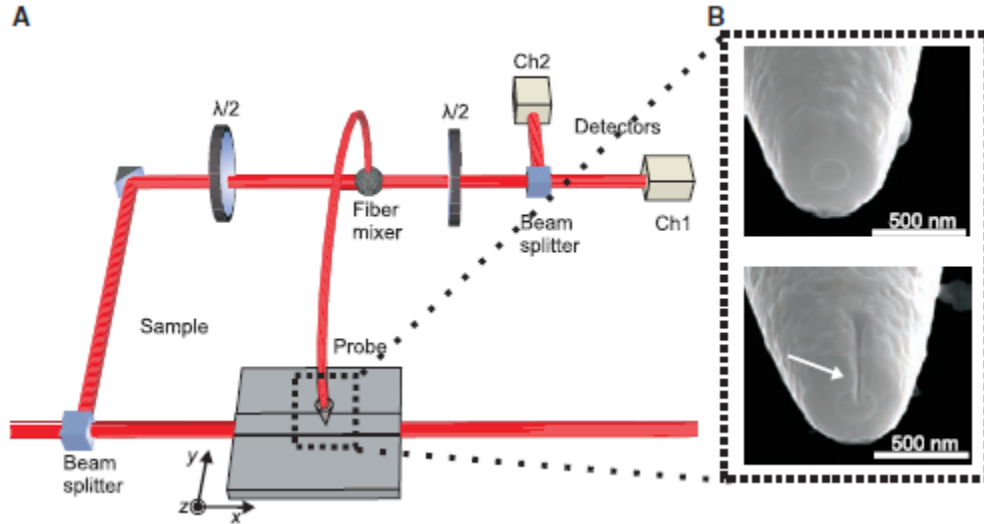


Figure 6: (a) Schematic of the experimental setup. (b) Scanning electron micrographs of the two probes used during experimentation – one cylindrical with aperture and the other showing an air gap emanating from the aperture [28].

2.3. Instrumental limitations

At optical frequencies, it is still very difficult with the current technology to measure the electric and magnetic field components of the electromagnetic wave directly versus real time as one cannot easily measure amplitudes and phases within one wavelength. The near-field optical spectroscopy and field mapping suffer from the electromagnetic coupling between the samples and the metallic measuring tip of the apparatus. This implies that the optical response is likely to be distorted [30]. The ability to use far-field techniques to optically detect nanostructures is therefore of great importance for performing measurements unaltered by the influences of test fixtures and measurement instruments.

Therefore the frequency-domain based far-field techniques are primarily employed. Usually, grating spectrometers or Fourier-transform spectrometers merely deliver the intensity of light versus wavelength or frequency. However, all phase information is lost here. Using interferometric techniques, phase information can be (partially) recovered. Commercially available ellipsometers promise to deliver optical constants of thin-film samples but in fact measure angle resolved reflectance polarisation data and rely on idealised models to retrieve the optical constants. Extreme caution should be exercised at this point, because the built-in post-processing software employed for analyzing (or, more precisely, interpreting) these data is limited to the models of dielectric materials and layered structures only. But it is usually inapplicable to deal with magnetic responses (or negative refractive indices). Also, analysis of the low symmetry of metamaterial samples can be problematic here too.

Due to the small lateral footprint of typical samples limited by the present fabrication processes, the incident light wave needs to be spot focused onto the specimen. If the source illuminates the sample edges and surrounding area, the measurement data will be contaminated by response of the other materials in the system. Once a lens is introduced, it concentrates the light from the lens aperture onto the sample at the expense of averaging over the half angular width of the sample seen from the lens aperture (defined as the numerical aperture, NA). This clearly introduces an undesired spread of the incident wave vector components of light, i.e., the experimental results are effectively averaged over a certain range of incidence angles, obviously leading to obscured data. The impact of that averaging process depends on the specific metamaterial under study. For example, it is quite common to image the samples by means of a microscope. As large

spectral bandwidths have to be investigated often, reflective microscope objectives are mandatory in order to avoid chromatic aberrations that would otherwise occur for glass-based lenses. It is well known that such Cassegrain objective lenses essentially cut out the normal incidence contribution and average over a cone of incidence angles (e.g., between 15° and 30° with respect to the surface normal for a numerical aperture of $NA = 0.5$). Again, the impact of these “artefacts” needs to be evaluated for each metamaterial structure separately. A sample that matches the source and detector areas and an arrangement that ensured all the scattered light is collected would constitute an ideal measurement.

Measuring broadband intensity transmittance and reflectance spectra with incident circular polarization of light is far from a trivial task. Broadband linear polarisers are readily available in most spectral ranges and a quarter-wave plate can turn this linear polarization into circular polarization. However, a usual quarter-wave plate has obvious inherent wavelength dependence. At optical and near-infrared frequencies, so-called super-achromatic quarter-wave plates are commercially available. At mid-infrared frequencies, such super-achromatic quarter-wave plates have to be custom-made that incurs significant cost. Also, these structures cannot always be easily integrated into existing (commercial) instrumentation setups. At THz and microwave frequencies, to our knowledge, such super-achromatic quarter-wave plates are presently unavailable at all.

3. State-of-the-art in experimental characterisation of nanostructured metamaterials

All experiments published to date have been far away from the ideal conceptual arrangements described in Section 2.1. Several different techniques are usually adopted for the experimental characterisation of metamaterials. The typical approaches are overviewed here.

3.1. Structures with inversion symmetry along the surface normal

Suppose that the metamaterial structure exhibits *inversion symmetry* along the surface normal. In this case, at normal incidence, the reflectance and transmittance spectra do *not* depend on which side of the sample is illuminated. A quite common procedure is to measure transmittance intensity and/or reflectance spectra of a metamaterial slab of thickness L for normal incidence of light and for two relevant (i.e., linearly independent) incident polarizations, either linear or circular. Clearly, these data containing two quantities at each wavelength are insufficient to retrieve uniquely the optical parameters, e.g., the complex refractive index and the complex impedance of the equivalent isotropic slab at each wavelength. Thus, usually, the experimental data are compared with the theoretical calculations for the designed specimen using additional information on the geometrical parameters which are obtained from optical and/or electron micrographs of the metamaterial samples. If sufficiently good agreement between experiment and theory is achieved, one may apply the theory to obtain the missing phase information.

One way of further *analyzing/interpreting* the experimental data is to model a fictitious slab of thickness L (with or without substrate) that has exactly the same complex reflectance and transmittance spectra as those of the metamaterial specimen. This “retrieval” procedure (see, e.g., review [3] for discussion of selecting the proper branches of non-unique solutions arising in this process) delivers the two complex quantities for the *effective* refractive index and impedance, or, equivalently, the *effective* complex dielectric permittivity and magnetic permeability of the slab. While this procedure is fairly well defined and broadly adopted in many laboratories around the world, one should be cautious in *interpreting* these retrieved quantities. Namely, they do represent the optical properties of the metamaterial slab with thickness L – yet they do not necessarily constitute the “material” properties in the conventional sense. One might be tempted to take the knowledge from normal optical materials and transfer it to metamaterials. For example, if one followed the retrieval procedure described above for a thin film of silica (SiO_2) of thickness L , it is clear that the measurements of the same film but of thickness $2L$ would give

nearly identical material parameters. This is *not* (!) necessarily the case for metamaterials. Generally, (near-field optical) interactions between different functional layers of the metamaterial can alter the *effective* “material parameters”. Whether or not this is a significant effect needs to be evaluated for each metamaterial structure under investigation – there is simply no universal answer. Two published experiments at optical frequencies that have addressed this issue [10], [12], and have come to the conclusion that these interaction effects are not too strong for their conditions (both are several layers of double fishnet negative-index metamaterials). A striking counter-example is in ref. [11], where the strong coupling between adjacent layers of split-ring resonators has qualitatively altered the properties of a single layer. Yet, the answer to this question also depends on how strongly the layer proximity influences the structure response. For example, it is known from (dielectric) photonic crystals that, for certain aspects (e.g., slow group velocities), the slab thickness exceeding even 100 lattice cells may be insufficient to reproduce the behaviour predicted by the band structure calculations for the fictitious infinite “material”.

3.2. Structures with no centre of inversion along the surface normal

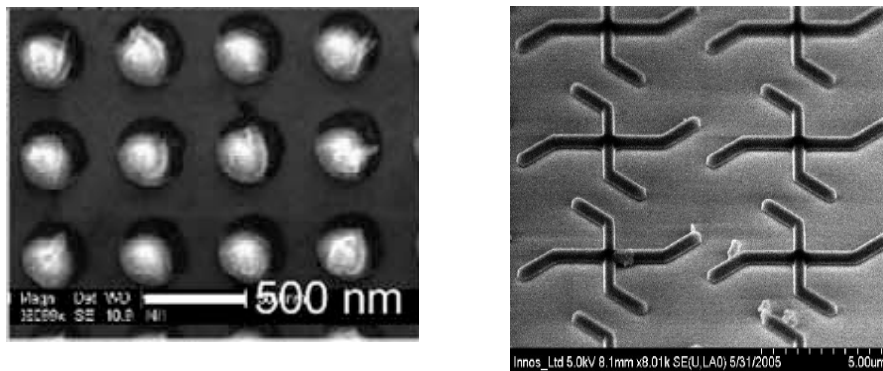


Fig. 7: (a) – a metamaterial with the centre of inversion (a multilayer array of plasmonic nanospheres prepared in nanogrooves). (b) – a metamaterial with no centre of inversion (a multilayer array of gammadion-shaped slots performed in the nanofilm of noble metal. Every nanofilm is placed on a dielectric substrate).

The situation becomes more complex if the metamaterial structure has *no centre of inversion* along the propagation direction of light. Such a metamaterial is shown in Fig. 7 in contrast to a spatially symmetric metamaterial. Still restricting ourselves to *normal incidence of light* onto the metamaterial slab, the complex transmittance and reflectance spectra are no longer the same for the two opposite directions of incidence. In other words, generally eight different quantities have to be measured at each wavelength – provided that the polarization state of the incident light is conserved in both reflectance and transmittance. Otherwise, the number of independent optical parameters doubles. In case of reciprocal structures (i.e., no static magnetic bias applied and no natural magnetic phase), the complex transmittances are strictly identical for both directions of propagation, whereas the respective complex reflection coefficients may differ. This amounts to six parameters at each wavelength. Again, in the published experiments, not the full fields but only the corresponding intensities have been measured. As a result, the problem of the *effective parameters*’ retrieval is underdetermined. As discussed in Section 3.1, additional theoretical input is required for extracting the effective optical parameters. One possible approach here is to retrieve the two complex impedances for each side of the equivalent slab at opposite directions of incident waves and a single complex refractive index. Alternatively, the complex permittivity and permeability as well as the bi-anisotropy parameter can be retrieved. Experimentally, this has been done in the literature only once so far in [31]. Needless to say that the meaning of these quantities is subject of the same constraints as in Section 3.1, i.e., caution has to be exercised in interpreting these effective quantities as the “material” parameters. They do, however, have a well

defined physical meaning for the measured film of thickness L . A variant of the latter approach is proposed in [32] to replace the bi-anisotropy parameter by a wave-vector dependence of permittivity and/or permeability.

3.3. Interferometric experiments

Additional information can be obtained from normal-incidence *interferometric experiments* that – at least partly – recover the missing phase information discussed above. Corresponding publications include Refs. [4], [33]-[35]. These additional inputs provide further sensitive tests of the level of agreement between the experiment and theory. In that sense, they are very important. However, these additional experimental data do not at all change the conceptual issues outlined in Section 3.1.

3.4. Oblique incidence

The situation becomes even more complex at *oblique incidence of light* onto the metamaterial slab. For usual optical materials, generally all optical quantities become tensors of rank two. Only very few experiments on metamaterials at optical frequencies have analysed oblique incidence of light [36]-[37]. These papers have just reported the measured transmittance intensity and/or reflectance spectra at different inclination and azimuth angles, but the authors have completely refrained from interrelating these measurement data to the effective “material” parameters. Theoretical aspects of the respective retrieval procedures are addressed in the literature, see, e.g., [38]-[39].

3.5. Chiral metamaterials

Lately, progress has been made in manufacturing uniaxial chiral metamaterials operating at microwave frequencies [40], THz frequencies [41], and optical frequencies [42]. Chiral structures are a subclass of bi-anisotropic structures. In bi-anisotropic structures, magnetic-dipole moments can be excited by the electric-field component of the light field and vice versa. In contrast to the general case of bi-anisotropy, where, e.g., the magnetic-dipole moments and the exciting electric field can be inclined at any angle, they are parallel in the case of chirality. This leads to a pure rotation of any incident linear polarised of light, i.e., to optical activity.

In refs. [40], [41] effective material parameters have actually been retrieved from the normal-incidence experimental data, while in ref. [42] different approach was employed. A detailed theoretical explanation of how the effective parameters can be retrieved from measured data has explicitly been given in Ref. [43]. Notably it was found that in contrast to the general bi-anisotropic case, reflectance and absorbance here do not depend on which side of the sample they are taken under normal incidence. Notice, that the structure shown in Fig. 7 is chiral though the scatterers (bianisotropic slots in the nanofilm) are planar and as such have no asymmetry along the normal direction. The chirality appears here due to the near-field interaction between the scatterer and its dielectric substrate (it vanishes if the substrate thickness tends to zero).

The results of [40], [41] have been discussed in a publication aiming at a broad general readership in ref. [44] (also see references cited therein). An interesting aspect of these latest results is that, for sufficiently strong chirality, a negative phase velocity of light can be obtained even if, in principle, the dielectric permittivity and the magnetic permeability are positive at the same time.

Provided that phase information is acquired (see above), the measurements can be performed equivalently either with linear or with circular polarization of the incident light. In Ref. [40], phase-sensitive transmittance and reflectance spectra have been obtained with linear polarization of the incident light. In Ref. [41], phase sensitive time-resolved data have been Fourier transformed. In both cases, data have to be acquired for different linear polarizations as three complex parameters (dielectric permittivity, magnetic permeability, and chirality parameter need to be retrieved). If no phase information is obtained (i.e., only intensity measurements combined with

the theory), a minimum requirement for a meaningful parameter retrieval is that one checks that the two incident circular polarizations of light stay circular (with the same handedness) upon transmission. Furthermore, from the generalized Fresnel coefficients it follows that left-handed circular polarization has to turn into right-handed circular polarization and vice versa in reflection. In other words, circular polarization cross-conversion needs to be small. This is equivalent to stating that the structures must not exhibit additional linear birefringence. This condition has not been fulfilled in Ref. [42], hence a chirality parameter could not be (and has not been) correctly retrieved.

More recent experimental work [45] has attempted to bring the structures of Ref. [40] (albeit with some modifications and simplifications) towards optical frequencies. Here, circular polarization conversion has been negligible and a maximum difference of the circular refractive indices of about 0.34 has been retrieved [45]. This difference is twice the chirality parameter. Both indices, however, have remained positive throughout the entire spectral range. Still, such structures are interesting and relevant as the optical activity obtained is rather broadband (about 100-nm bandwidth at around 1360-nm center wavelength) and many orders of magnitude larger than what is obtained from, e.g., solutions containing chiral sugar molecules [45].

3.6. On measurements of the effective refractive index

In order to somewhat justify the use of the *effective* refractive index, n , of metamaterials made of stacked layers of periodic inclusions, convergence of the retrieved value of n when increasing the number of layers has been studied experimentally in [12]. The observed convergence rate of n proved to be consistent with the findings of the theoretical paper [46] based on a similar double-fishnet type negative-index photonic metamaterial design. Ref. [46] reports convergence for four functional layers. However, one should be aware that these quantities are not the fundamental physical parameters at all. Increasing the spacing between adjacent functional layers of the double-fishnet structure will decrease their coupling (see discussion in Section 3.1). As a result, convergence can even be achieved for a single functional layer [47]. Inferring other optical parameters (e.g., permittivity or permeability) from such refraction experiments [12] again requires making use of the dedicated theoretical models of the measured specimens.

An alternative type of the refraction measurements is based upon the use of prism made of wedge-shaped metamaterial sample (rather than the slabs discussed so far). The light wave transmitted through such samples is generally deflected due to refraction. Measuring the corresponding light deflection angles allows the refractive index to be inferred from Snell's law. However, such obtained refractive index is generally differ from the refractive index n usually referred to in connection with the phase velocity of light, c , in material being slower by factor n than the vacuum speed of light, c_0 , i.e., $c=c_0/n$. A brief discussion of this issue can be found, e.g., in ref. [48]. The experiments addressing the change in the direction of the Poynting vector (energy flow) have been published [9]. The samples investigated in [9] were fabricated via evaporation of a stack of 21 alternating layers of silver and dielectric (corresponding to 10 lattice cells). Next, holes were drilled using focused-ion-beam (FIB) lithography to obtain a stacked fishnet type structure. Finally, a wedge which forms a prism has been produced, again using FIB lithography. The measured wavelength-dependent changes in beam direction have been compared with the time-domain simulations in CST Microwave Studio. The simulation and measurement results for the real part of the refractive index are in qualitative agreement. And on this basis the authors have concluded that ten functional layers (lattice cells) suffice for the retrieved *effective* refractive index to be representative of the "bulk" material. However, the same calculations *disagree* with the experimental data by a factor larger than five for the imaginary part of the refractive index, i.e., the maximal measured figure of merit of about 3 is much smaller than the calculated value of about 20.

Different approach to retrieval of the metamaterial parameters has been presented in ref. [49]. The high-resolution spectral method based on Bloch-wave symmetry properties was applied experimentally to extracting mode dispersion in periodic waveguides. The technique is based

upon the measurements and mapping of near-field profiles. Both the travelling and evanescent modes were taken into account, and the amplitudes of forward and backward waves in different waveguide configurations were determined with the estimated uncertainty of several percents or less. Whereas the commonly employed Spatial Fourier-Transform (SFT) analysis provides the wavenumber resolution which is limited by the inverse length of the waveguide, the precise dispersion characteristic extraction has been achieved even for compact photonic structures. While the measurement concept is generally applicable to arbitrary frequencies, the experimental results have been presented only in the microwave range. The examples of periodic dielectric waveguide, artificial transmission line and overmoded dielectric slab waveguide have illustrated robustness of the developed approach to retrieval of the dispersion characteristics by mapping the field distributions.

4. Concluding Remarks

Optical metamaterials, because of their typically limited area and number of functional layers, are more easily understood as finite structures with interfaces that define their optical behaviour. This definition is in contrast to a conventional material in which their bulk properties define their optical properties. The retrieved 'material' parameters are the subject of interpretation unless the samples have sufficient extent in the measurement direction to suppress the interface effects. Also the phase information is harder to obtain giving the need for either more sophisticated measuring tools, such as time domain or interference methods, or alternatively, more complex structures, i.e. phase masks made with the metamaterial.

The current challenges and difficulties of characterization of nanostructured materials have been summarised in [50] where the author stated that "...as we near the one hundred year mark since the birth of crystallography, we face a resilient frontier in condensed matter physics: our inability to routinely and robustly determine the structure of complex nanostructured and amorphous materials. ... Yet what has become clear with the emergence of nanotechnology is that diffraction data alone may not be enough to uniquely solve the structure of nanomaterials". Commenting on the recent paper [51] which presented the approach to determination of the structure of complex nanostructured materials, the author argued that the major challenges arise from the limited information content of the measurement data along with the growing complexity of the models used for data post-processing. Uniqueness of the associated inverse problems is a real issue, as is the availability of good nanostructure solution algorithms. Additional constraints coming from prior knowledge about the system, or additional data sets, from different information sources are required to constrain a unique solution for retrieval of the material parameters. The author of [50] suggests: "We may be relearning lessons from crystallography... These constraints are just common sense, but place enormous restrictions on the solution space and the efficiency and uniqueness of solutions. Nanostructure solution is much younger than crystallography, but the field is rapidly growing up."

References

- [1] V.M. Shalaev, *Nature Photon.* **1**, 41 (2007).
- [2] C.M. Soukoulis, S. Linden, and M. Wegener, *Science* **315**, 47 (2007).
- [3] K. Busch, G. von Freymann, S. Linden, S. Mingaleev, L. Tkeshelashvili, and M. Wegener, *Phys. Rep.* **444**, 101 (2007).
- [4] S. Zhang, W. Fan, N.C. Panoiu, K.J. Malloy, R.M. Osgood, and S.R.J. Brueck, *Phys. Rev. Lett.* **95**, 137404 (2005).
- [5] N. Feth, C. Enkrich, M. Wegener, and S. Linden, *Opt. Express* **15**, 501 (2007)
- [6] W. Wu, E. Kim, E. Ponizovskaya, Z. Liu, Z. Yu, N. Fang, Y.R. Shen, A.M. Bratkovsky, W. Tong, C. Sun, X. Zhang, S.-Y. Wang and R.S. Williams, *Appl. Phys. A* **87**, 143 (2007).
- [7] J. H. Lee, Q. Wu, and W. Park, Metal nanocluster metamaterial fabricated by the colloidal self-assembly, *Optics Letters*, Vol. 34, Issue 4, pp. 443-445 (2009)

- [8] J. A. Fan, C. Wu, K. Bao, J. Bao, R. Bardhan, N.J. Halas, V.N. Manoharan, P. Nordlander, G. Shvets, F. Capasso, Self-Assembled Plasmonic Nanoparticle Clusters, *Science*, Vol. 328. no. 5982, pp. 1135 - 1138, May 2010.
- [9] K. Lodewijks, N. Verellen, W. Van Roy, G.f Borghs, P. Van Dorpe, Self-assembled hexagonal double fishnets as negative index materials, Preprint arXiv:1010.5138v1, Oct. 2010.
- [10] G. Dolling, M. Wegener, and S. Linden, *Opt. Lett.* **32**, 551 (2007).
- [11] N. Liu, H. Guo, L. Fu, S. Kaiser, H. Schweizer, and H. Giessen, *Nature Mater.* **7**, 317 (2008).
- [12] J. Valentine, S. Zhang, T. Zentgraf, E. Ulin-Avila, D. A. Genov, G. Bartal, X. Zhang, *Nature*, **455**, 376 (2008); doi:10.1038/nature07247.
- [13] H. J. Lezec, J.A. Dionne, and H. Atwater, *Science* **316**, 430 (2007).
- [14] S. Burgos, R. de Waele, A. Polman, H. Atwater, *Nature Materials* **9**, 407-412 (2010)
- [15] M. W. Klein, C. Enkrich, M. Wegener, C. M. Soukoulis, and S. Linden, "Single-slit split-ring resonators at optical frequencies: limits of size scaling," *Opt. Lett.* **31**(9), 1259–1261 (2006)
- [16] Nanostructured Metamaterials, Exchange between experts in electromagnetics and materials science, Ed Anne F de Baas, Luxembourg, European Union 2010 ISBN 978-92-79-07563-6
- [17] F. Hesmer, E. Tatartschuk, O. Zhuromskyy, A. A. Radkovskaya, M. Shamonin, T. Hao, C. J. Stevens, G. Faulkner, D. J. Edwards, and E. Shamonina, "Coupling mechanisms for split ring resonators: Theory and experiment," *Phys. Status Solidi* **244**(4), 1170–1175 (2007)
- [18] N. Liu, S. Kaiser, and H. Giessen, "Magnetoinductive and Electroinductive Coupling in Plasmonic Metamaterial Molecules," *Adv. Mater.* **20**(23), 4521–4525 (2008)
- [19] http://en.wikipedia.org/wiki/Fourier_transform_infrared_spectroscopy, visited 13/10/2010
- [20] http://en.wikipedia.org/wiki/File:Ellipsometry_setup.svg, visited 13/10/2010
- [21] (See chapter 3) Novel Techniques in THz-Time-Domain-Spectroscopy, A comprehensive study of technical improvements to THz-TDS Matthias Hofmann Inaugural-Dissertation Fakultät für Mathematik und Physik der Albert-Ludwigs-Universität Freiburg im Breisgau vorgelegt von Stefan Gorenflo aus Hausen im Wiesental im November 2006
- [22] E. Pshenay-Severin, F. Setzpfandt, C. Helgert, U. Hübner, C. Menzel, A. Chipouline, C. Rockstuhl, A. Tünnermann, F. Lederer, and T. Pertsch *J. Opt. Soc. Am. B*, **27**, No. 4/ pp 660-666 April 2010
- [23] J. Han, "Probing negative refractive index of metamaterials by terahertz time-domain spectroscopy", *Optics Express*, **16**, no. 2, pp. 1354 – 1364 (2008).
- [24] S. Ha, A. A. Sukhorukov, K.B. Dossou, L.C. Botten, C. Martijn de Sterke, and Y.S. Kivshar, "Bloch-mode extraction from near-field data in periodic waveguides," *Opt. Lett.* **34**, 3776-3778 (2009)
- [25] N. Feth, M. König, M. Husnick, K. Stannigel, J. Niegemann, K. Busch, M. Wegener, S. Linden, *Optics Express* **18**(7), 6545, 2010
- [26] A. Arbouet, D. Christofilos, N. Del Fatti, F. Vallee, J. Huntzinger, L. Arnaud, P. Billaud, M. Broyer, *Phys. Rev. Lett.* **93**(12), 127401, 2004
- [27] A. Bitzer, H. Merbold, A. Thoman, T. Feurer, H. Helm, and M. Walther, "Terahertz near-field imaging of electric and magnetic resonances of a planar metamaterials", *Optics Express*, Vol. 17, Issue 5, pp. 3826-3834, 2009
- [28] M. Buresi, D. van Oosten, T. Kampfrath, H. Schoenmaker, R. Heideman, A. Leinse, and L. Kuipers, "Probing the Magnetic Field of Light at Optical Frequencies", *Science* 23 October 2009: 326 (5952), 550-553.
- [29] D. Diessel, M. Decker, S. Linden, and M. Wegener, "Near-field optical experiments on low-symmetry split-ring-resonator arrays", *Optics Letters*, Vol. 35, Issue 21, pp. 3661-3663, 2010.
- [30] A. Liu, A. Rahmani, G. W. Bryant, L.J. Richter, and S.J. Stranick, "Modeling illumination-mode near-field optical microscopy of Au nanoparticles", *JOSA A*, Vol. 18, Issue 3, pp. 704-716, 2001.
- [31] M.S. Rill, C. Plet, M. Thiel, I. Staude, G. von Freymann, S. Linden, and M. Wegener, *Nature Mater.* **7**, 543 (2008).
- [32] A.R. Bungay, Yu.P. Svirko, and N. Zheludev, *Phys. Rev. B* **47**, 11730 (1993).
- [33] V.M. Shalaev, W. Cai, U.K. Chettiar, H. Yuan, A.K. Sarychev, V.P. Drachev, and A.V. Kildishev, *Opt. Lett.* **30**, 3356 (2005).
- [34] G. Dolling, C. Enkrich, M. Wegener, C.M. Soukoulis, and S. Linden, *Science* **312**, 892 (2006).
- [35] G. Dolling, M. Wegener, C.M. Soukoulis, and S. Linden, *Opt. Lett.* **32**, 53 (2007).

- [36] C. Enkrich, M. Wegener, S. Linden, S. Burger, L. Zschiedrich, F. Schmidt, J. Zhou, T. Koschny, and C.M. Soukoulis, *Phys. Rev. Lett.* **95**, 203901 (2005).
- [37] G. Dolling, M. Wegener, A. Schädle, S. Burger, S. Linden, *Appl. Phys. Lett.* **89**, 231118 (2006).
- [38] R. Marqués, F. Medina, and R. Rafii-El-Idrissi, *Phys. Rev. B* **65**, 144440 (2002).
- [39] X. Chen, B.-I. Wu, J.A. Kong, and T.M. Grzegorzcyk, *Phys. Rev. E* **71**, 046610 (2005).
- [40] E. Plum, J. Zhou, J. Dong, V. A. Fedotov, T. Koschny, C. M. Soukoulis and N. I. Zheludev, *Phys. Rev. B* **79**, 035407 (2009)
- [41] S. Zhang, Y.-S. Park, J. Li, X. Lu, W. Zhang, X. Zhang, *Phys. Rev. Lett.* **102**, 023901 (2009)
- [42] N. Liu, H. Liu, S. Zhu, and H. Giessen, *Nature Photon.* **3**, 157 (2009)
- [43] D.H. Kwon, D. H. Werner, A. V. Kildishev, and V. M. Shalaev, *Opt. Express* **16**, 11822 (2008)
- [44] M. Wegener and S. Linden, *Physics* **2**, 3 (2009)
- [45] M. Decker, M. Ruther, C. Kriegler, J. Zhou, C. M. Soukoulis, S. Linden, and M. Wegener, *Opt. Lett.*, submitted (2009)
- [46] C. Rockstuhl, T. Paul, F. Lederer, T. Pertsch, T. Zentgraf, T. P. Meyrath, and H. Giessen, *Phys. Rev. B* **77**, 035126 (2008)
- [47] C.M. Soukoulis et al., unpublished (2008)
- [48] M. Wegener, G. Dolling, and S. Linden, *Nature Mater.* **6**, 475 (2007).
- [49] A. A. Sukhorukov, Sangwoo Ha, I. V. Shadrivov, D. A. Powell, and Y. S. Kivshar, *Opt. Express* **17**, 3716 (2009)
- [50] S.J.L. Billinge, "The nanostructure problem" *Physics* **3**, 25 (2010), DOI: 10.1103/Physics.3.25
- [51] M. J. Cliffe, M. T. Dove, D. A. Drabold, and A. L. Goodwin, "Structure Determination of Disordered Materials from Diffraction Data", *Phys. Rev. Lett.* **104**, 125501 (2010)